inorganics

MDPI

Article

Supramolecular Organization of Diaryliodonium Dicyanoargentates(I) Provided by Iodine(III)–Cyanide Halogen Bonding

Irina S. Aliyarova [1], Anastasiia V. Koziakova [1], Daniil M. Ivanov [1,*], Natalia S. Soldatova [2] and Pavel S. Postnikov [2]

[1] Institute of Chemistry, Saint Petersburg State University, Universitetskaya Nab. 7/9, Saint Petersburg 199034, Russia; i.aliyarova@spbu.ru (I.S.A.); nas.lofflas@gmail.com (A.V.K.)
[2] Research School of Chemistry and Applied Biomedical Sciences, Tomsk Polytechnic University, Tomsk 634034, Russia; soldatovans@tpu.ru (N.S.S.); postnikov@tpu.ru (P.S.P.)
* Correspondence: d.m.ivanov@spbu.ru

Abstract: Three diaryliodonium dicyanoargentates(I), [MesIAr][Ag(CN)$_2$] (Ar = Ph **1**, Mes **2**, 4-MeC_6H_4 **3**; Mes = 2,4,6-$Me_3C_6H_2$), were prepared by anion metathesis. The X-ray structural analyses for these crystals revealed C–I^{III}···N≡C halogen bonds (abbreviated as XB) between I atoms of diaryliodonium cations and N atoms of cyano groups, which provide different supramolecular organization. The noncovalent nature of these interactions was studied by density functional theory (DFT) calculations and topological analysis of the electron density distribution in the framework of the quantum theory of atoms in molecules (QTAIM) at the PBE-D3/jorge-DZP-DKH level of theory both in gas phase and crystal models. The philicities of partners in these contacts were confirmed by electron localization function (ELF) projections, electron density/electrostatic potential (ED/ESP) profiles, and Hirshfeld surfaces analysis. An analysis of the available crystallographic data from the literature allows us to find other examples of σ-hole interactions including the dicyanoargentate(I) anion, and the C–X···N≡C (X = Br, I, Te) bonding were also confirmed theoretically.

Keywords: diaryliodonium; dicyanoargentate(I); halogen bonding; crystal engineering

check for updates

Academic Editor: Michael A. Beckett

Received: 8 April 2025
Revised: 5 May 2025
Accepted: 7 May 2025
Published: 9 May 2025

Citation: Aliyarova, I.S.; Koziakova, A.V.; Ivanov, D.M.; Soldatova, N.S.; Postnikov, P.S. Supramolecular Organization of Diaryliodonium Dicyanoargentates(I) Provided by Iodine(III)–Cyanide Halogen Bonding. *Inorganics* **2025**, *13*, 157. https://doi.org/10.3390/inorganics13050157

Copyright: © 2025 by the authors. Licensee MDPI, Basel, Switzerland. This article is an open access article distributed under the terms and conditions of the Creative Commons Attribution (CC BY) license (https://creativecommons.org/licenses/by/4.0/).

1. Introduction

Halogen bonding [1] (XB) is a type of σ-hole interaction [2,3] that has applications in catalysis [4–6], biochemistry [7–10], the molecular design of luminescent materials [11,12], the stabilization of explosive compounds [13,14], and supramolecular chemistry [15,16]. The nature of halogen bonds varies from ionic to coordinative [17,18].

Among the typical XB donors, the IUPAC definition [1] also mentions iodonium cations. Due to the positive charge and two σ-holes [19], they tend to form charge-supported interionic XBs in the solid state, which was realized even with such a low-nucleophilic counterion as $[AuCl_4]^-$ [20,21]. Due to the supramolecular organization based on diaryliodonium cations, it is possible to form both isolated [20,22–24], most often heterotrameric clusters [20,24–27], and more complex polymeric 1D chains [20,25,27–29] and 2D layers [27,29].

Dicyanoargentate(I) is an actively studied building block in supramolecular chemistry. It is involved in the formation of supramolecular polymers [30–33], including compounds

with variable magnetic properties [34–38]. Isolated dicyanoargentate(I) is capable of forming hydrogen [39–43] and argentophilic $Ag^{I}\cdots Ag^{I}$ interactions between the dicyanoargentates(I), themselves providing dimeric [44], trimeric [45], and even polymeric [46,47] aggregation. Polymer aggregation also occurs during interionic charge-supported argentophilic interactions in $[L_2Ag][Ag(CN)_2]$ (L = 1,3-dibutyl-1H-benzo[d]imidazol-2-ylidene), as well as in cation-anionic heterometallophilic $Ag^{I}\cdots Au^{I}$ in $[L_2Au][Ag(CN)_2]$ (L = 1,3-dimethyl-1H-benzo[d]imidazol-2-ylidene) [48] and $Ag^{I}\cdots Pt^{II}$ interactions in the structures of $[PtL_4][Ag(CN)_2]_2$ (L_4 = $(NH_3)_4$; $(H_2NCH_2CH_2NH_2)_2$) [42,43]. Klapötke et al. [49] described the structures of $[R_3Te][Ag(CN)_2]$ (R = Me, Ph), which, along with the argentophilic $Ag^{I}\cdots Ag^{I}$ interactions between the anions, exhibit short Te···N contacts between dicyanoargentate(I) and telluronium cations. The authors characterized these contacts as secondary interactions, whereas, according to modern concepts and in accordance with their geometric characteristics, they can be classified as charge-supported chalcogen bonds [50].

Our inspection of CCDC data revealed two structures with possible Br···N (refcode SADYAZ) and I···N (YIHDEB) XBs involving a dicyanoargentate anion. For the first case [51], only the presence of contact has been mentioned, but the nature of the interactions has not been analyzed in any way. For the I···N contact [52], the authors indicated the linear geometry of the interaction and also discussed its nature, highlighting all the characteristics of a halogen bond. However, the interaction was not classified as a halogen bond. Thus, a systematic study of XBs involving dicyanoargentate(I) has not been conducted, although for analogous dicyanoaurate(I) the I···N XBs have been described [53].

Previously, we evaluated halogen bonds involving metallates [20,21,23,24,54] with a particular focus on square-planar tetracyanometallates (Ni, Pd, Pt) [28,55] using diaryliodonium cations as XB donors. As a continuation of these studies, in this contribution, we synthesized a series of diaryliodonium dicyanoargentates(I) $[MesIAr][Ag(CN)_2]$ (Ar = Ph **1**, 4-MeC_6H_4 **2**, Mes **3**; Mes = 2,4,6-$Me_3C_6H_2$). According to the single crystal X-ray structural analysis and subsequent theoretical calculations, interionic C–$I^{III}\cdots$N≡C–Ag XBs were identified in these structures, which led to different supramolecular assemblies, depending on the shape of the cation.

2. Results and Discussion

2.1. Identification of Structure-Directing Noncovalent Interactions

A series of diaryliodonium dicyanoargentates(I) $[MesIAr][Ag(CN)_2]$ (Ar = Ph **1**, Mes **2**, 4-MeC_6H_4 **3**; Mes = 2,4,6-$Me_3C_6H_2$) was synthesized by metathesis from corresponding diaryliodonium triflates. In all cases, X-ray diffraction experiments revealed the formation of the interionic C–I···N≡C–Ag interactions, which can be interpreted as XBs according to their geometrical parameters (Figures 1–3). Note that only one example of diaryliodonium argentate(I), $[(o\text{-}C_6H_4)_2I]_3[Ag(OTf)_4]$ [56], was previously synthesized and analyzed using single-crystal X-ray diffraction and theoretical calculations.

In **1**–**3**, the I···N distances are significantly shorter than the Bondi van der Waals radii [57] sum (d(I···N) = 2.843(3)–3.067(3) Å vs. $\sum_{vdw}$(I + N) = 3.53 Å), and the C–I···N angles (from 168.00(8) to 176.97(9)°) were close to 180°. According to these geometrical parameters and considering the IUPAC criteria for XB [1], all of the I···N interactions can be interpreted as XB—the geometric parameters of all XBs are shown in Table 1. In **1**, the formation of the C7–I1···N2A≡C2A XB may have caused the distortion of the linear C_{sp} environment in the corresponding cyanide ligand (∠(N2A≡C2A–Ag1A = 173.6(2)°).

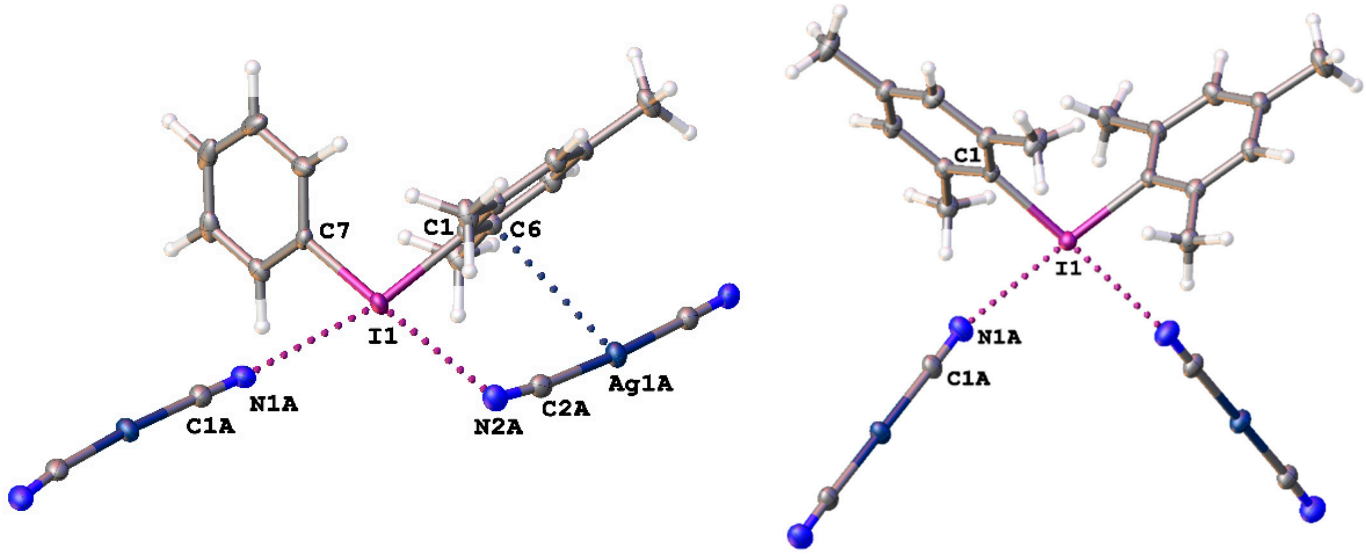


Figure 1. Heterotrimeric fragments in the structures of **1** and **2** (from **left** to **right**) illustrating the C–I^{III}···N≡C–Ag XBs and the Ag···C interactions, which are given by dotted lines. Thermal ellipsoids are at the 50% probability level.

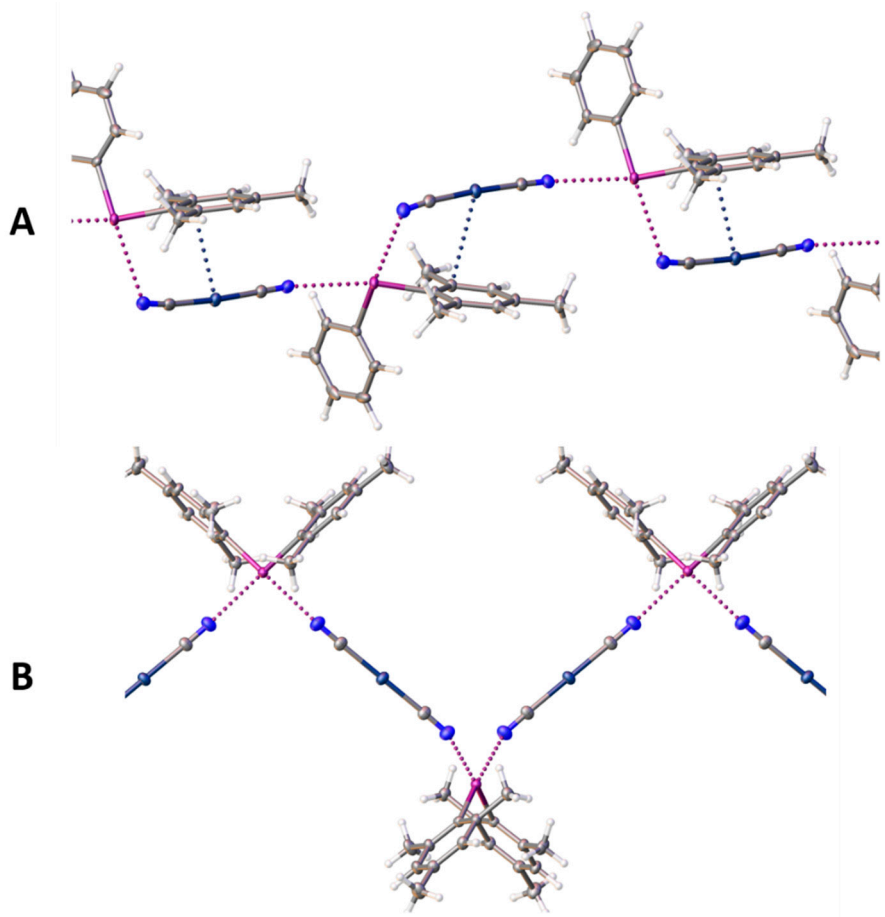


Figure 2. Representation (Olex2-1.5) of infinite chains in the structure of **1** (**A**) and **2** (**B**). XBs and Ag···C interactions are assigned as dotted lines. Color codes: gray, carbon; off-white, hydrogen; blue, nitrogen; violet, iodine; dark-blue, silver.

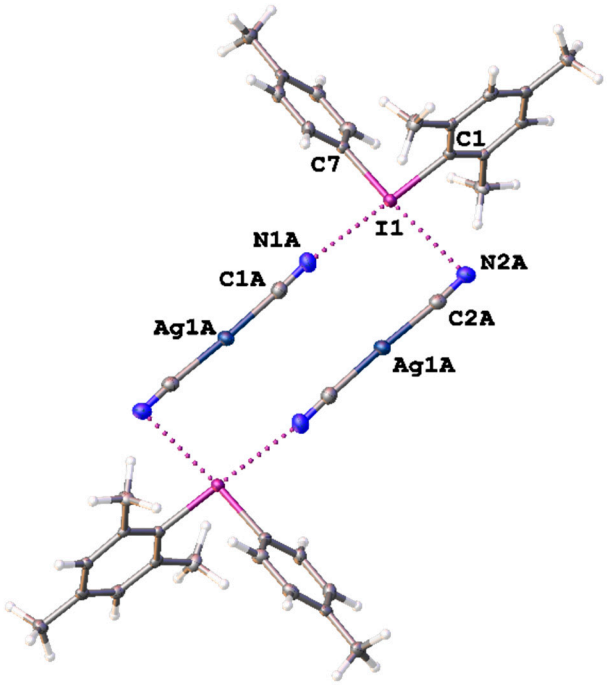


Figure 3. Heterotetrameric aggregation in the structure of **3**. The C–I^{III}···N≡C–Ag XBs are given by dotted lines, and thermal ellipsoids are at the 50% probability level.

Table 1. Parameters of the C–I···N XBs.

Structure	Contact	d(I···N), Å	ΣvdW	Nc *	∠(C–I···N), °	∠(C≡N···I), °
1	C1–I1···N1A≡C1A	2.993(3)	3.53	0.85	168.00(8)	154.00(15)
	C7–I1···N2A≡C2A	3.033(2)	3.53	0.86	174.19(8)	100.85(18)
2	C1–I1···N1A≡C1A	2.843(3)	3.53	0.81	175.13(11)	148.7(3)
3	C1–I1···N1A≡C1A	2.894(3)	3.53	0.82	176.97(9)	165.2(2)
	C7–I1···N2A≡C2A	3.067(3)	3.53	0.87	174.24(8)	92.0(2)

* The normalized contact (Nc) is defined as the ratio between the separation observed in the crystal and the sum of Bondi van der Waals radii of interacting atoms: $Nc = d/\Sigma_{vdW}$; $\Sigma_{vdW}(I + N) = 3.53$ Å.

Comparable I···N XBs were previously reported for diaryliodonium salts with square-planar tetracyanonickelates(II), tetracyanopalladates(II), and tetracyanoplatinates(II) (2.768(3)–2.936(2) Å) [28,55], and for square-planar tetracyanoaurates(III) with fulvalene-based cations [58,59] (2.83(1)–3.28(1) Å). Related I···N XBs were also found in iodopyridinium [60] salts with $[M(CN)_6]^{3-}$ (M = Cr, Fe, Co) with 2.789(7)–3.116(7) Å distance range and with protonated [61] hexacyanoferrates(II) (3.12(4)–3.81(4) Å), and between C_2I_2 and tetracyanonickelates(II) (2.768(3)–2.955(3)Å) [62] or hexacyanoferrates(III) (2.710(4)–3.021(8) Å) [63].

Due to the presence of these XBs, two types of supramolecular aggregates (Figure 2) were formed: infinite chains (in the case of structures **1**–**2**) and a 4-membered heterotetramer (for structure **3**). Such aggregation has been previously described for diaryliodonium salts with another pseudohalide ligand, i.e., the thiocyanate anion. The formation of 2D chains was investigated previously [25] in the structure of dibenziodolium thiocyanate. In a previous article [26], I···N and I···S XBs were described and theoretically confirmed for acyclic diaryliodonium salts, which lead to heterotetrameric aggregation.

2.2. Hirshfeld Surface Analysis

To verify the type of noncovalent forces that contributed to crystal packing, we performed Hirshfeld surface analysis (HSA) on the XRD structures of **1**–**3**. The HSA (Figure 4), as expected, indicated the domination of the contacts involving H and C atoms because their fraction is large; the major contributions of intermolecular contacts to HSA are shown in Table S2 (Supplementary Materials). The contribution of I···N intermolecular contacts to Hirshfeld surfaces was also significant (2.6–2.7%). Since the I···N XBs are the most interesting in the context of this work, they are extensively discussed in Section 3.1.

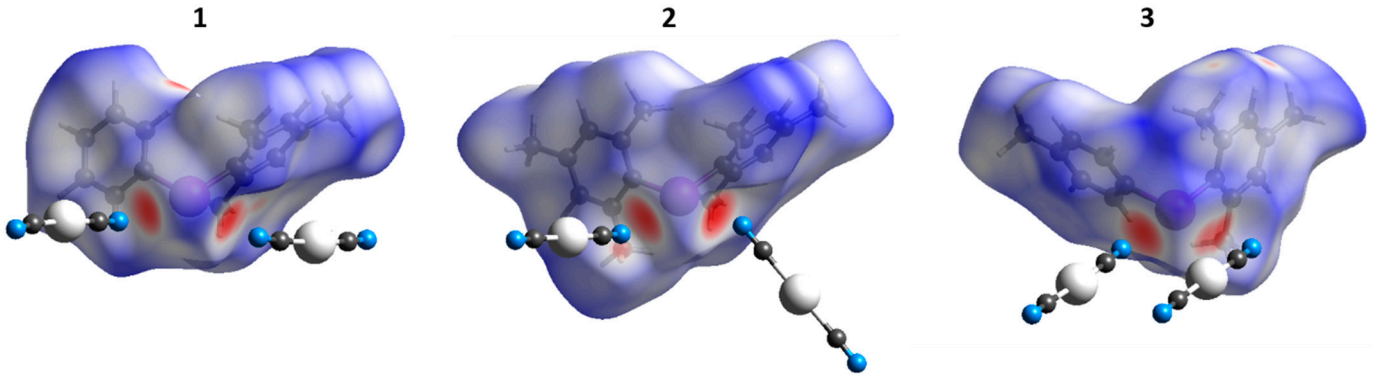


Figure 4. Hirshfeld surfaces for the XRD structure of **1**–**3**; contacts shorter than the sum of van der Waals radii are shown in red, longer contacts in blue.

2.3. Theoretical Considerations

To understand the nature of the main structure-directing noncovalent interactions, we performed DFT calculations (PBE-D3/jorge-DZP-DKH with Douglas–Kroll–Hess 2nd order scalar relativistic calculations) based on the experimentally determined coordinates for heterotrimer (from **1** or **2**) or heterotetramer (from **3**) supramolecular clusters or for crystal models with periodic boundary conditions (with GAPW method [64]). The existence and noncovalent nature of the interactions were confirmed by QTAIM topological analysis. The nucleophilicity of nitrogen centers and electrophilic role of iodine atoms in diaryliodonium cations in the identified XBs were studied using a set of independent methods, including ELF projections and ED/ESP profiles.

The QTAIM analysis for both cluster and crystal models demonstrated the presence of bond critical points (3, −1) (BCPs) between iodine and nitrogen atoms in all cases (Table 2). The negative and small values of the sign $(\lambda_2)\rho$ on the other BCPs confirmed the attractive and noncovalent nature of the interactions [65]. They can also be considered as noncovalent interactions due to their close to zero positive energy density (0.000–0.002 Hartrees/Bohr^3) and the balance of the Lagrangian kinetic energy G(**r**) and the potential energy density V(**r**) (−G(**r**)/V(**r**) > 1) on the corresponding BCPs [66]. Note that all I···N BCP parameters for crystal and cluster models were equal.

Table 2. Parameters in (3, −1) bond critical points (the electron density with sign of λ_2 sign(λ_2)ρ(**r**) in e/Bohr^3, Laplacian of electron density $\nabla^2\rho$(**r**) in e/Bohr^5, local electronic energy density H_b, local electronic potential energy density V(**r**), and local electronic kinetic energy density G(**r**) in Hartree/Bohr^3) corresponding to the C–I···N interactions in the **1**–**3** crystals and (PhIMes$^+$)·(Ag(CN)$_2$)$_2$ (from **1**), (Mes$_2$I$^+$)·(Ag(CN)$_2$)$_2$, (from **2**), and (MesI(4-MeC$_6$H$_4$)$^+$)$_2$·(Ag(CN)$_2$)$_2$ (from **3**) clusters.

Structure	Bond	Model	sign(λ_2)ρ(r)	$\nabla^2\rho$(r)	G(r)	V(r)	H_b
1	C1–I1···N1A	crystal	−0.020	0.059	0.014	−0.013	0.001
		cluster	−0.020	0.059	0.014	−0.013	0.001
	C7–I1···N2A	crystal	−0.017	0.054	0.012	−0.011	0.001
		cluster	−0.017	0.054	0.012	−0.011	0.001
2	C1–I1···N1A	crystal	−0.027	0.073	0.019	−0.019	0.000
		cluster	−0.027	0.073	0.019	−0.019	0.000
3	C1–I1···N1A	crystal	−0.024	0.069	0.017	−0.017	0.000
		cluster	−0.024	0.069	0.017	−0.017	0.000
	C7–I1···N2A	crystal	−0.016	0.054	0.012	−0.010	0.002
		cluster	−0.016	0.054	0.012	−0.010	0.002

2.3.1. Electron Localization Function (ELF) Projections

To confirm that the observed I···N contacts belonged to the XB, we performed the electron localization function (ELF) [67–69] projections in combination with QTAIM analysis for the crystal models of **1**–**3** (Figure 5).

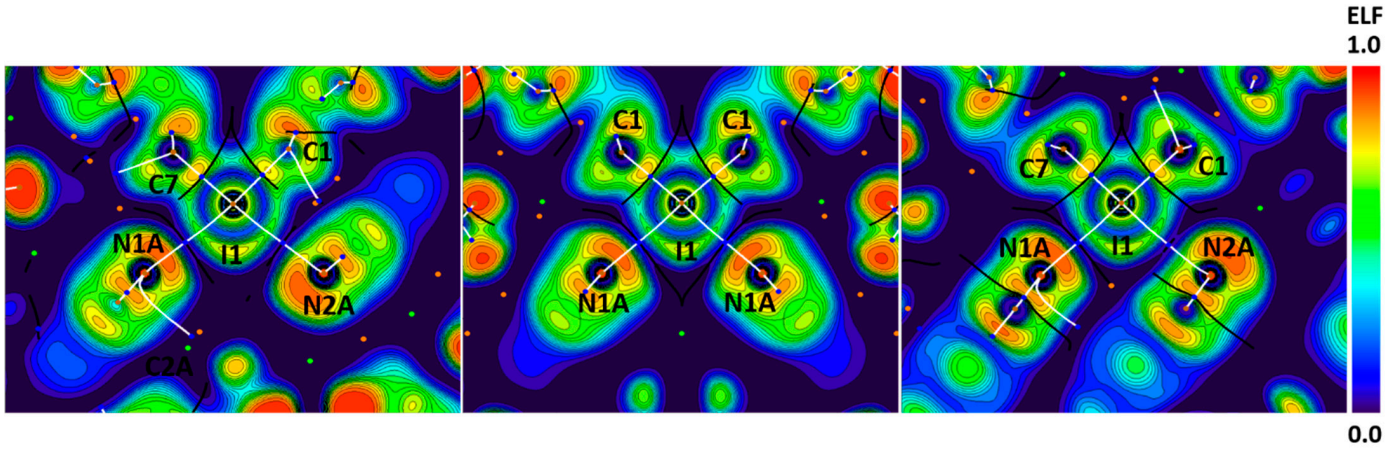


Figure 5. Visualization of ELF, BCPs, and bond paths for C–I···N XBs in the crystals of **1**–**3**. BCPs (3, −1) are shown in blue; nuclear critical points (3, −3) are shown in pale brown; ring critical points (3, +1) are shown in orange; bond paths are shown as white lines.

The I···N bond paths pass through the areas between lone and shared pairs of iodine atoms, which confirms the electrophilic nature of iodine atoms toward nitrogen atoms in these interactions. However, in the cases of the C≡N···I angles around 90°, bond paths pass outside the orange N lone pair areas and the nitrogen nucleophilicity provided by π-C≡N electrons. This leads to weaker and longer XBs (Figure 5, Table 1) with lower ρ values in BCPs (0.016–0.017 vs. 0.020–0.027 e/Bohr^3 in other cases).

2.3.2. ED/ESP Profiles

Additional information about the nature of interacting atoms in noncovalent interactions can be obtained by the analysis of the order of the ED (electron density) and ESP

(electrostatic potential) minima in their 1D profiles along the bond path [70–75]. According to the analyses, the ESP minimum should shift toward the nucleophilic atom, while the ED minimum is closer to the electrophilic atom. The ED/ESP profiles along the I···N bond paths in $(PhIMes^+)\cdot(Ag(CN)_2)_2$, (from **1**), $(Mes_2I^+)\cdot(Ag(CN)_2)_2$, (from **2**) and $(MesI(4\text{-}MeC_6H_4))_2\cdot(Ag(CN)_2)_2$ (from **3**) clusters indicated (Figure 6) that the ESP minima shifted to the N ρ-basin. In all considered cases, this shift could be interpreted as the nucleophilicity of the nitrogen center toward the iodine atom.

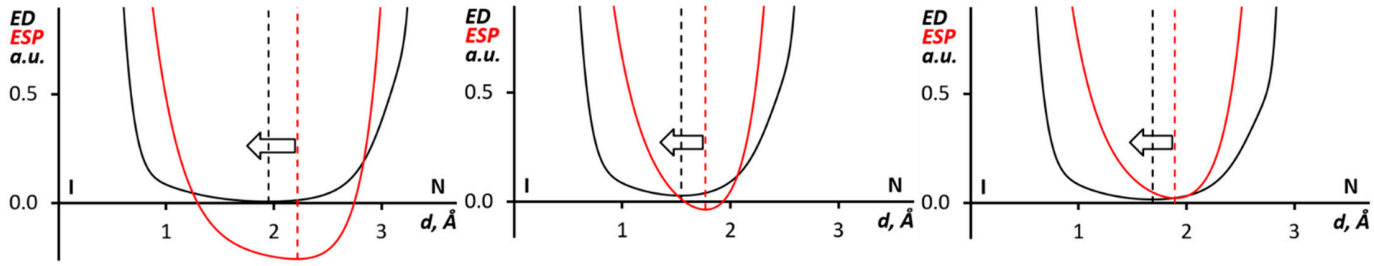


Figure 6. The ED (black) and ESP (red) 1D profiles along the I···N bond paths for the $(PhIMes^+)\cdot(Ag(CN)_2)_2$ (from **1**, **left** panel), $(Mes_2I^+)\cdot(Ag(CN)_2)_2$, (from **2**, **center** panel), and $(MesI(4\text{-}MeC_6H_4))_2\cdot(Ag(CN)_2)_2$ (from **3**, **right** panel) clusters.

In addition, using this method, we studied the Ag···C interaction between silver(I) atoms of dicyanoargentate(I) anion and π-system of diaryliodonium cation, which was confirmed by QTAIM analysis. Parameters in the corresponding BCP ($\text{sign}(\lambda_2)\rho(\mathbf{r}) = -0.007$ e/Bohr^3, $\nabla^2\rho(\mathbf{r}) = 0.021$ e/Bohr^5, $G(\mathbf{r}) = 0.004$ Hartree/Bohr^3, $V(\mathbf{r}) = -0.003$ Hartree/Bohr^3) showed the purely noncovalent nature of the interaction [65,66]. As shown in Figure 7, the ED and ESP minimums almost coincide which makes it possible to interpret this interaction as quasi-metallophilic [76].

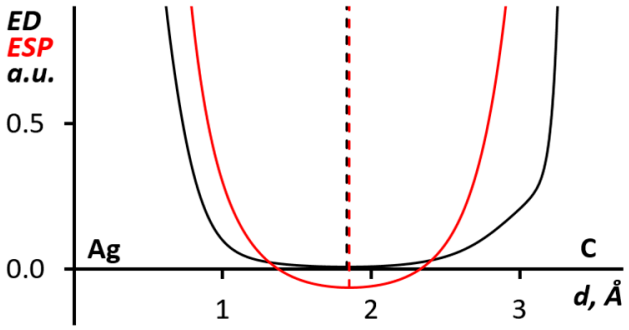


Figure 7. The ED (black) and ESP (red) 1D profiles along the Ag···C bond paths for the $(PhIMes^+)\cdot(Ag(CN)_2)_2$ (from **1**) cluster.

2.4. Dicyanoargetates(I) in Other σ-Hole Interactions

As mentioned in the Introduction, $[Ag(CN)_2]^-$ can also form Te···N chalcogen bonds (ChB) together with argentophillic interactions Ag···Ag in the crystal structure of $[Ph_3Te][Ag(CN)_2]$ (Figure 8, CSD refcode: HUHCES) [49]. However, the authors of the article only mentioned the Te···N interactions and labeled them secondary. Theoretical calculations confirming the nature of these contacts were also not carried out.

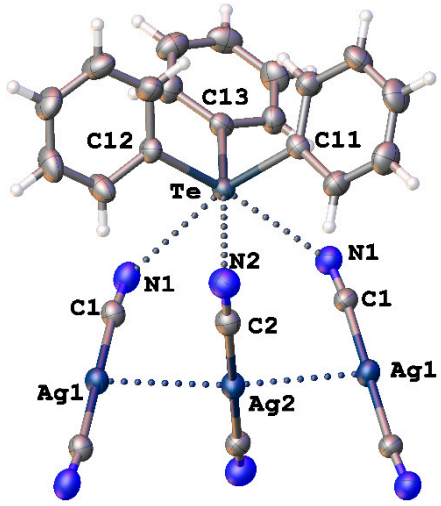


Figure 8. Heterotetrameric fragment from structure of $[Ph_3Te][Ag(CN)_2]$ (CSD refcode: HUHCES).

In addition, we found two structures in which the $[Ag(CN)_2]^-$ anion was involved in the formation of XBs. In the structure of $[IEDT]_2[Ag(CN)_2]$ (IEDT = iodoethylenedithiotetrathiafulvalene and -fulvalenium) (CSD refcode: YIHDEB), strong interionic I···N interactions were described where they are formed between a nitrogen atom of dicyanoargentate(I) anion and an iodine atom of the corresponding cation (Figure 9) [52].

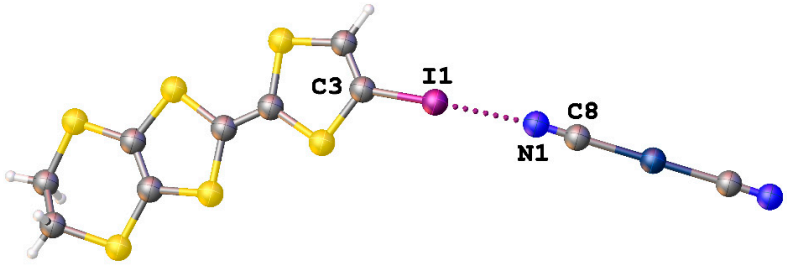


Figure 9. The I···N interaction in the structure of $[IEDT]_2[Ag(CN)_2]$ (CSD refcode: YIHDEB).

Mallah and coworkers [51] observed Br···N short contacts in the structure of $(C_{11}H_{20}BrN_2)[Ag(CN)_2)]$ (CSD refcode: SADYAZ) (Figure 10). But the nature of both of these contacts was not discussed in corresponding articles, and they were not attributed to XBs.

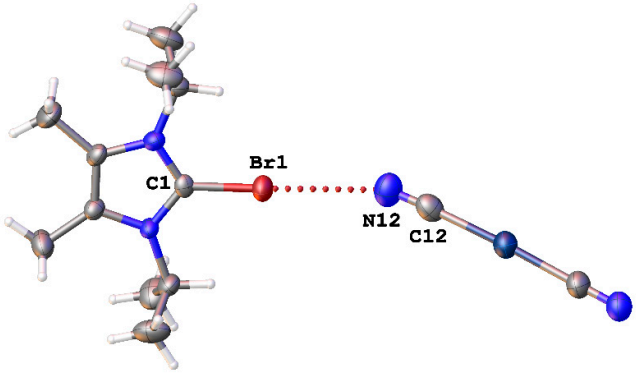


Figure 10. The Br···N interaction in the structure of $(C_{11}H_{20}BrN_2)[Ag(CN)_2)]$ (CSD refcode: SADYAZ).

Since the nature of these interactions was not studied by the authors of the relevant articles, we carried out theoretical calculations for all the presented structures with

periodic boundary conditions in the PBE-D3/jorge-DZP-DKH level of theory with Douglas–Kroll–Hess 2nd order scalar relativistic calculations in the GAPW method. The results of the QTAIM topological analysis can be found in Table 3. The calculated BCP values of sign(λ_2)ρ(**r**) were found to be small and negative, indicating that the nature of the corresponding interactions was attractive and noncovalent.

Table 3. Parameters in (3, −1) bond critical points (the electron density with sign of λ_2 sign(λ_2)ρ(**r**) in e/Bohr^3, Laplacian of electron density $\nabla^2\rho$(**r**) in e/Bohr^5, local electronic energy density H_b, local electronic potential energy density V(**r**), and local electronic kinetic energy density G(**r**) in Hartree/Bohr^3) corresponding to the C–I···N and Ag···Ag interactions in the YIHDEB, SADYAZ, and HUHCES crystals.

System	Bond	d(X···Y), Å	sign(λ_2)ρ(r)	$\nabla^2\rho$(r)	G(r)	V(r)	H_b
YIHDEB	C3–I1···N1	2.876(5)	−0.023	0.070	0.017	−0.017	0.000
SADYAZ	C1–Br1···N12	2.959(8)	−0.014	0.054	0.011	−0.008	0.003
HUHCES	C12–Te···N1	3.162(5)	−0.013	0.042	0.009	−0.008	0.001
	C11–Te···N1	3.346(5)	−0.009	0.031	0.006	−0.005	0.001
	C13–Te···N2	3.501(5)	−0.008	0.025	0.005	−0.004	0.001
	Ag···Ag	2.98470(6)	−0.026	0.031	0.013	−0.019	−0.006

We established the attractive nature and the nucleophilic character of the nitrogen atom in $[Ag(CN)_2]^-$ by appropriate theoretical calculations. In the case of Te···N contacts in the structure of HUHCES, bond paths passed between the Te lone pair areas and through the lone pair areas of the N atoms or through the π-bonding areas of cyanide of the dicyanoargentate(I) on their ELF projections (Figure 11). Thus, there is evidence of electrophilicity of the tellurium atom toward the cyanide ligand.

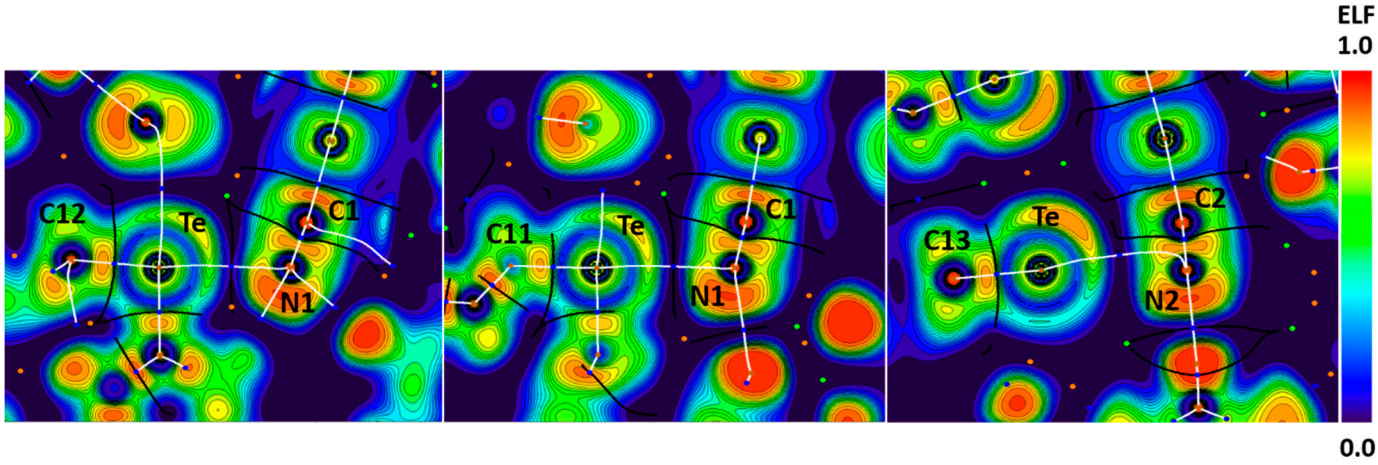


Figure 11. Visualization of ELF, BCPs, and bond paths for C–Te···N (left pannel) ChBs in the crystal of HUHCES. BCPs (3, −1) are shown in blue; nuclear critical points (3, −3) are shown in pale brown; ring critical points (3, +1) are shown in orange; bond paths are shown as white lines.

In the structures of YIHDEB and SADYAZ, the X···N (X = I, Br) bond path passes through the areas with high ELF values on the N atom and thoroughly depleted ELF regions on the X atoms. This gives evidence favoring the nucleophilicity of nitrogen atoms in these interactions (Figure 12). Thus, both the I···N and Br···N contacts can be interpreted as XBs.

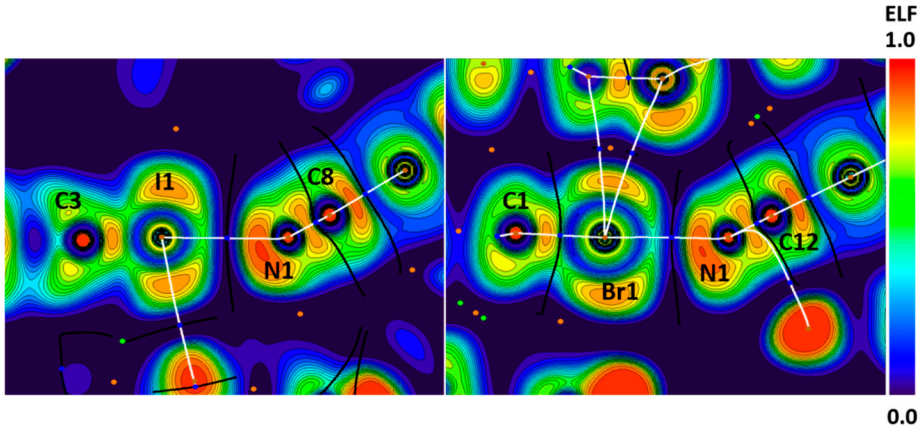


Figure 12. Visualization of ELF, BCPs, and bond paths for C–I···N (**left** panel) and C–Br···N (**right** panel) XBs in the crystals of YIHDEB and SADYAZ, respectively. BCPs (3, −1) are shown in blue; nuclear critical points (3, −3) are shown in pale brown; ring critical points (3, +1) are shown in orange; bond paths are shown as white lines.

3. Materials and Methods

3.1. General Information

Solvents and $K[Ag(CN)_2]$ (Sigma Aldrich (Merck, Darmstadt, Germany)) were obtained from commercial sources and used as received. The diaryliodonium triflates were prepared by the known method [77].

The NMR spectra were recorded on Bruker AVANCE III 400 and Bruker AVANCE 500 spectrometers (Billerica, MA, USA) at ambient temperature in acetone-d6 or $CDCl_3$ (at 500 or 400, 126 or 101 MHz for ^1H, $^{13}C\{^1H\}$, respectively) (Figures S10–S15). IR spectra (Figures S7–S9) were recorded on a Bruker (Billerica, MA, USA) TENSOR 27 FT-IR spectrometer (4000–400 cm^{-1}, KBr pellets). The HRESI-MS data (Figures S4–S6) were obtained on a "MaXis", Bruker Daltonik GmbH (Billerica, MA, USA), and Shimadzu Nexera X2 LCMS-9030 (Shimadzu Corp., Japan, Kyoto) spectrometers equipped with an electrospray ionization (ESI) source; CH_2Cl_2 was used as a solvent.

3.2. Synthesis and Characterization of Diaryliodonium Dicyanoargentates(I)

Diaryliodonium dicyanoargentates **1**–**3** were prepared in good yields (64–84%) via ligand metathesis. A concentrated aqueous solution of $K[Ag(CN)_2]$ was added to methanolic solution of the corresponding diaryliodonium triflate [77] in a 1:5 molar ratio. The resulting white precipitate was washed with water (3 × 10 mL) and hexane (3 × 10 mL), followed by centrifugation. The final products were dried in the air. In **1**–**3**, both types of cations were identified by high-resolution ESI-MS and additionally characterized by ^1H and $^{13}C\{^1H\}$ NMR and IR spectroscopies. Single-crystal X-ray diffraction (SC XRD) studies were performed for all three compounds (Figures 1–3).

Crystals of **1**–**3** were obtained by the crystallization of the synthetized complexes either from CH_2Cl_2/Et_2O (**1**) or MeOH (**2**, **3**) solutions, with full details as follows:

Mesityl(phenyl)iodonium dicyanoargentate (1). Yield: 78% (23.9 mg), mp: 147–148 °C (dec.). $HRESI^+$-MS (MeOH, *m*/*z*): 323.0288 ($[M - Ag(CN)_2]^+$, calcd 323.0291; $HRESI^-$-MS (MeOH, *m*/*z*): 158.9114 ($[M - C_{15}H_{16}I]^-$, calcd 158.9118. IR (KBr, selected bonds, cm^{-1}): 2924 ν(C–H), 2123 ν(C≡N), 1563 (s) $\nu(C_{ar}–C_{ar})$, 1443 δ(C–H), 743 $\delta(C_{ar}–H)$, 450 (s) ν(C–I). ^1H NMR (500 MHz, Chloroform-d) δ 7.67 (m, 2H), 7.57 (m, 1H), 7.44 (m, 2H), 7.14 (s, 2H), 2.64 (s, 6H), 2.39 (s, 3H). $^{13}C\{^1H\}$ NMR (126 MHz, Chloroform-d) δ 146.72, 145.28, 142.44, 133.40, 132.85, 132.43, 131.16, 27.70, 21.63. The crystals suitable for XRD study were obtained by slow evaporation of CH_2Cl_2/Et_2O solution at RT in air.

Dimesityliodonium dicyanoargentate (2). Yield: 64% (32.4 mg), mp: 169–170 °C (dec.). HRESI$^+$-MS (MeOH, m/z): 365.0767 ([M − $Ag(CN)_2$]$^+$, calcd 365.0761; HRESI$^-$-MS (MeOH, m/z): 158.9115 ([M − $C_{18}H_{22}I$]$^-$, calcd 158.9118. IR (KBr, selected bonds, cm^{-1}): 2924 ν(C–H), 2139 ν(C≡N), 1589 (s) ν(C_{ar}–C_{ar}), 1456 δ(C–H), 756 δ(C_{ar}–H), 542 (s) ν(C–I). ^{1}H NMR (400 MHz, Acetone-d6) δ 7.26 (s, 4H), 2.60 (s, 12H), 2.36 (s, 6H). ^{13}C {^{1}H} NMR (101 MHz, Acetone-d6) δ 144.87, 143.33, 142.63, 131.71, 118.74, 26.22, 20.84. Compound **2** was crystallized from methanol at RT in air.

Mesityl(*p*-tolyl)iodonium dicyanoargentate (3). Yield: 84% (27.5 mg), mp: 146–147 °C (dec.). HRESI$^+$-MS (MeOH, m/z): 337.0450 ([M − $Ag(CN)_2$]$^+$, calcd 337.0448); HRESI$^-$-MS (MeOH, m/z): 158.9115 ([M − $C_{16}H_{18}I$]$^-$, calcd 158.9118). IR (KBr, selected bonds, cm^{-1}): 2924 ν(C–H), 2126 ν(C≡N), 1455 (s) ν(C_{ar}–C_{ar}), 1378 δ(C–H), 797 δ(C_{ar}–H), 479 (s) ν(C–I). ^{1}H NMR (500 MHz, Chloroform-d) δ 7.57 (d, J = 8.4 Hz, 2H), 7.23 (d, J = 8.4 Hz, 2H), 7.12 (s, 2H), 2.64 (s, 6H), 2.39 (s, 3H), 2.38 (s, 3H). ^{13}C {^{1}H} NMR (126 MHz, Chloroform-d) δ 146.24, 144.85, 143.34, 142.04, 133.43, 133.40, 130.85, 122.08, 108.94, 27.42, 21.49, 21.34. Compound **3** was crystallized from methanol at RT in air.

3.3. X-Ray Structure Determinations

For single-crystal XRD experiments, crystals of **1**–**3** were fixed on a micro mount and placed on SuperNova, Dual, Cu at home/near, Atlas and SuperNova diffractometers (Agilent Technologies, Santa Clara, CA, USA), Single source at offset/far, and HyPix3000 (Rigaku Holdings Corporation, Tokyo, Japan) diffractometers, respectively, and measured at 100 K using MoKα monochromated radiation. The structures were solved by the Superflip [78–80] and the ShelXT [81] structure solution programs using Charge Flipping and Intrinsic Phasing and refined by means of the ShelXL program [81] incorporated in the OLEX2 program package [82]. H atoms in all structures were placed in ideal calculated positions according to neutron diffraction statistical data [83] and refined as colliding atoms with parameters of relative isotropic displacement. The crystal data and structures refinements are collected in Table S1. CCDC 2428066, 2428070, and 2428069 contain the supplementary crystallographic data for this paper.

3.4. Computational Details

Before calculations, structures YIHDEB, SADYAZ, and HUHCES were equipped with H atoms placed in ideal calculated positions accordingly to neutron diffraction statistical data [83] using the OLEX2 program package [82].

Single-point DFT calculations under periodic boundary conditions (*crystal* models) for all studied crystals (1 × 1 × 2 cell for YIHDEB or 1 × 1 × 1 cell for all other cases) were conducted in the CP2K-8.1 program [84–90], with 350 plane wave, 50 Ry relative plane wave cutoffs for the auxiliary grid using the PBE-D3 [91–93] level of theory and the Gaussian/augmented plane wave (GAPW) method [64] with a full-electron jorge-DZP-DKH [94–97] atomic-centered basis set with the Douglas–Kroll–Hess 2nd-order scalar relativistic calculations with requested relativistic core Hamiltonian [98,99]. The 1.0×10^{-6} Hartree convergence was achieved for the self-consistent field cycle in the Γ-point approximation. The starting fractional coordinates were shifted along one (along ***c*** for HUHBUH) or two (along ***a*** and ***b*** for 1 × 1 × 2 cell for YIHDEB) of the translation vectors by 0.5 to move the atoms participating in interactions under consideration to the center of the cell. Multiplicity was set to 2 for YIHDEB and to 1 for all other cases.

Single-point calculations for the (PhIMes$^+$)·$(Ag(CN)_2)_2$, (from **1**), (Mes_2I^+)·$(Ag(CN)_2)_2$, (from **2**), and (MesI(4-MeC_6H_4))$_2$·$(Ag(CN)_2)_2$ (from **3**) clusters were performed based on their experimental X-ray geometries at the DFT level of theory using the PBE-D3 [91–93]/jorge-

DZP-DKH [94–97] with Douglas–Kroll–Hess 2nd order scalar relativistic calculations [98] with the help of Gaussian-09 [100] program package.

The topological analysis of the electron density distribution, with the help of the quantum theory of atoms in molecules (QTAIM) method developed by Bader [101], ELF [67] projection analysis, and ED/ESP profile analysis [75] were performed using the Multiwfn program (version 3.8) [102].

The Hirshfeld surface analysis was carried out using the CrystalExplorer program [103–105]. The contact distances (d_{norm}), based on R_{vdW} [57], were mapped on the Hirshfeld surfaces. In the color scale, the negative values of d_{norm} were visualized in red, indicating contacts shorter than Σ_{vdW}. The values represented in white denoted the intermolecular distances close to the contacts with d_{norm} equal to zero. The contacts longer than Σ_{vdW} with positive d_{norm} values were colored in blue.

4. Conclusions

This study systematically demonstrated the critical role of halogen bonding (XB) in directing the supramolecular assembly of diaryliodonium dicyanoargentates(I). Theoretical analyses, including QTAIM, ELF projections, ED/ESP profiles, and Hirshfeld surfaces, confirmed the noncovalent nature of these interactions and the role of partners in these contacts. The studied XBs led to the formation of supramolecular architectures, resulting in the formation of infinite chains (**1**–**2**) or heterotetramers (**3**) depending on the steric effects of the cation. The coexistence of XBs and quasi-metallophilic Ag···C interactions highlighted the multifunctional potential of these systems in designing materials with tunable optoelectronic or catalytic properties.

This work increases the understanding of halogen bonding in metallate frameworks and shows the potential for exploiting σ-hole interactions, particularly the dicyanoargentate(I) anion, in supramolecular design.

Supplementary Materials: The following supporting information can be downloaded at: https://www.mdpi.com/article/10.3390/inorganics13050157/s1, Table S1: Crystal data and structure refinement for 1–3; Table S2: Results of HSA for the cationic parts in the X-ray structures of 1–3 obtained at 100(2) K; Figure S1: HRESI$^+$-MS of 1; Figure S2: HRESI$^-$-MS of 1; Figure S3: HRESI$^+$-MS of 2; Figure S4: HRESI$^-$-MS of 2; Figure S5: HRESI$^+$-MS of 3; Figure S6: HRESI$^-$-MS of 3; Figure S7: IR spectrum of 1; Figure S8: IR spectrum of 2; Figure S9: IR spectrum of 3; Figure S10: ^{1}H NMR spectrum of 1; Figure S11: ^{13}C NMR spectrum of 1; Figure S12: ^{1}H NMR spectrum of 2; Figure S13: ^{13}C NMR spectrum of 2; Figure S14: ^{1}H NMR spectrum of 3; Figure S15: ^{13}C NMR spectrum of 3; Figure S16: No Ag···Ag short contacts were found in all cases.

Author Contributions: I.S.A.—writing, investigation, and computational study; A.V.K.—syntheses and investigation, D.M.I.—writing, computational study, conceptualization, and project administration, N.S.S.—writing, P.S.P.—writing. All authors have read and agreed to the published version of the manuscript.

Funding: This research was funded by the Russian Science Foundation, grant number 24-73-00143.

Institutional Review Board Statement: Not applicable.

Informed Consent Statement: Not applicable.

Data Availability Statement: The original contributions presented in this study are included in the article/Supplementary Material. Further inquiries can be directed to the corresponding author.

Acknowledgments: The authors thank the resource centers of St. Petersburg State University "Centre for X-ray Diffraction Studies", "Chemical Analysis and Materials Research Centre", and "Magnetic Resonance Research Centre" for their support in the research.

Conflicts of Interest: The authors declare no conflicts of interest.

References

1. Desiraju, G.R.; Ho, P.S.; Kloo, L.; Legon, A.C.; Marquardt, R.; Metrangolo, P.; Politzer, P.; Resnati, G.; Rissanen, K. Definition of the Halogen Bond (IUPAC Recommendations 2013). *Pure Appl. Chem.* **2013**, *85*, 1711–1713. [CrossRef]
2. Brinck, T.; Murray, J.S.; Politzer, P. Surface Electrostatic Potentials of Halogenated Methanes as Indicators of Directional Intermolecular Interactions. *Int. J. Quantum Chem.* **1992**, *44*, 57–64. [CrossRef]
3. Mallada, B.; Gallardo, A.; Lamanec, M.; de la Torre, B.; Špirko, V.; Hobza, P.; Jelinek, P. Real-space Imaging of Anisotropic Charge of σ-hole by Means of Kelvin Probe Force Microscopy. *Science* **2021**, *374*, 863–867. [CrossRef]
4. Tepper, R.; Schubert, U.S. Halogen Bonding in Solution: Anion Recognition, Templated Self-Assembly, and Organocatalysis. *Angew. Chem. Int. Ed.* **2018**, *57*, 6004–6016. [CrossRef]
5. Benz, S.; Poblador-Bahamonde, A.I.; Low-Ders, N.; Matile, S. Catalysis with Pnictogen, Chalcogen, and Halogen Bonds. *Angew. Chem. Int. Ed.* **2018**, *57*, 5408–5412. [CrossRef]
6. Nandy, A.; Sekar, G. Dibenziodolium Salts as Halogen Bond Donor Catalysts for the Reduction of Quinolines, One-Pot Reductive Amination, and Addition Reaction with Indoles. *Eur. J. Org. Chem* **2022**, *2022*, e202200982. [CrossRef]
7. Auffinger, P.; Hays, F.A.; Westhof, E.; Ho, P.S. Halogen Bonds in Biological Molecules. *Proc. Natl. Acad. Sci USA* **2004**, *101*, 16789–16794. [CrossRef]
8. Costa, P.J.; Nunes, R.; Vila-Viçosa, D. Halogen Bonding in Halocarbon-Protein Complexes and Computational Tools for Rational Drug Design. *Expert Opin. Drug Discov.* **2019**, *14*, 805–820. [CrossRef]
9. Ho, P.S. Biomolecular Halogen Bonds. In *Halogen Bonding I: Impact on Materials Chemistry and Life Sciences*; Springer International Publishing: Cham, Switzerland, 2015; pp. 241–276. [CrossRef]
10. Berger, G.; Frangville, P.; Meyer, F. Halogen Bonding for Molecular Recognition: New Developments in Materials and Biological Sciences. *Chem. Comm.* **2020**, *56*, 4970–4981. [CrossRef]
11. Yan, D.; Evans, D.G. Molecular Crystalline Materials with Tunable Luminescent Properties: From Polymorphs to Multi-component Solids. *Mater. Horiz.* **2014**, *1*, 46–57. [CrossRef]
12. Sivchik, V.V.; Solomatina, A.I.; Chen, Y.-T.; Karttunen, A.J.; Tunik, S.P.; Chou, P.-T.; Koshevoy, I.O. Halogen Bonding to Amplify Luminescence: A Case Study Using a Platinum Cyclometalated Complex. *Angew. Chem.* **2015**, *54*, 14057–14060. [CrossRef]
13. Landenberger, K.B.; Bolton, O.; Matzger, A.J. Energetic–Energetic Cocrystals of Diacetone Diperoxide (DADP): Dramatic and Divergent Sensitivity Modifications via Cocrystallization. *J. Am. Chem. Soc.* **2015**, *137*, 5074–5079. [CrossRef]
14. Bennion, J.C.; Vogt, L.; Tuckerman, M.E.; Matzger, A.J. Isostructural Cocrystals of 1,3,5-Trinitrobenzene Assembled by Halogen Bonding. *Cryst. Growth Des.* **2016**, *16*, 4688–4693. [CrossRef]
15. Adonin, S.A.; Sokolov, M.N.; Fedin, V.P. Polyhalide-bonded Metal Complexes: Structural Diversity in an Eclectic Class of Compounds. *Coord. Chem. Rev.* **2018**, *367*, 1–17. [CrossRef]
16. Sonnenberg, K.; Mann, L.; Redeker, F.A.; Schmidt, B.; Riedel, S. Polyhalogen and Polyinterhalogen Anions from Fluorine to Iodine. *Angew. Chem. Int. Ed.* **2020**, *59*, 5464–5493. [CrossRef]
17. Wieske, L.H.E.; Erdelyi, M. Halogen Bonds of Halogen(I) Ions—Where Are We and Where to Go? *J. Am. Chem. Soc.* **2024**, *146*, 3–18. [CrossRef]
18. Rissanen, K.; Haukka, M. Halonium Ions as Halogen Bond Donors in the Solid State $[XL_2]Y$ Complexes. In *Halogen Bonding II: Impact on Materials Chemistry and Life Sciences*; Springer International Publishing: Cham, Switzerland, 2015; pp. 77–90. [CrossRef]
19. Cavallo, G.; Murray, J.S.; Politzer, P.; Pilati, T.; Ursini, M.; Resnati, G. Halogen Bonding in Hypervalent Iodine and Bromine Derivatives: Halonium Salts. *IUCrJ* **2017**, *4*, 411–419. [CrossRef]
20. Aliyarova, I.S.; Ivanov, D.M.; Soldatova, N.S.; Novikov, A.S.; Postnikov, P.S.; Yusubov, M.S.; Kukushkin, V.Y. Bifurcated Halogen Bonding Involving Diaryliodonium Cations as Iodine(III)-Based Double-σ-Hole Donors. *Cryst. Growth Des.* **2021**, *21*, 1136–1147. [CrossRef]
21. Aliyarova, I.S.; Tupikina, E.Y.; Soldatova, N.S.; Ivanov, D.M.; Postnikov, P.S.; Yusubov, M.; Kukushkin, V.Y. Halogen Bonding Involving Gold Nucleophiles in Different Oxidation States. *Inorg. Chem.* **2022**, *61*, 15398–15407. [CrossRef]
22. Soldatova, N.S.; Suslonov, V.V.; Kissler, T.Y.; Ivanov, D.M.; Novikov, A.S.; Yusubov, M.S.; Postnikov, P.S.; Kukushkin, V.Y. Halogen Bonding Provides Heterooctameric Supramolecular Aggregation of Diaryliodonium Thiocyanate. *Crystals* **2020**, *10*, 230. [CrossRef]
23. Suslonov, V.V.; Soldatova, N.S.; Ivanov, D.M.; Galmés, B.; Frontera, A.; Resnati, G.; Postnikov, P.S.; Kukushkin, V.Y.; Bokach, N.A. Diaryliodonium Tetrachloroplatinates(II): Recognition of a Trifurcated Metal-Involving μ_3-I···(Cl,Cl,Pt) Halogen Bond. *Cryst. Growth Des.* **2021**, *21*, 5360–5372. [CrossRef]
24. Semenov, A.V.; Baykov, S.V.; Soldatova, N.S.; Geyl, K.K.; Ivanov, D.M.; Frontera, A.; Boyarskiy, V.P.; Postnikov, P.S.; Kukushkin, V.Y. Noncovalent Chelation by Halogen Bonding in the Design of Metal-Containing Arrays: Assembly of Double σ-Hole Donating Halolium with Cu^{I}-Containing O,O-Donors. *Inorg. Chem.* **2023**, *62*, 6128–6137. [CrossRef] [PubMed]
25. Postnikov, P.S.; Guselnikova, O.A.; Yusubov, M.S.; Yoshimura, A.; Nemykin, V.N.; Zhdankin, V.V. Preparation and X-ray Structural Study of Dibenziodolium Derivatives. *J. Org. Chem.* **2015**, *80*, 5783–5788. [CrossRef] [PubMed]

26. Soldatova, N.S.; Postnikov, P.S.; Suslonov, V.V.; Kissler, T.Y.; Ivanov, D.M.; Yusubov, M.S.; Galmés, B.; Frontera, A.; Kukushkin, V.Y. Diaryliodonium as a Double σ-Hole Donor: The Dichotomy of Thiocyanate Halogen Bonding Provides Divergent Solid State Arylation by Diaryliodonium Cations. *Org. Chem. Front.* **2020**, *7*, 2230–2242. [CrossRef]
27. Radzhabov, A.D.; Ledneva, A.I.; Soldatova, N.S.; Fedorova, I.I.; Ivanov, D.M.; Ivanov, A.A.; Yusubov, M.S.; Kukushkin, V.Y.; Postnikov, P.S. Halogen Bond-Involving Self-Assembly of Iodonium Carboxylates: Adding a Dimension to Supramolecular Architecture. *Int. J. Mol. Sci.* **2023**, *24*, 14642. [CrossRef]
28. Suslonov, V.V.; Soldatova, N.S.; Postnikov, P.S.; Resnati, G.; Kukushkin, V.Y.; Ivanov, D.M.; Bokach, N.A. Diaryliodonium Tetracyanidometallates Self-Assemble into Halogen-Bonded Square-Like Arrays. *Cryst. Growth Des.* **2022**, *22*, 2749–2758. [CrossRef]
29. Soldatova, N.S.; Suslonov, V.V.; Ivanov, D.M.; Yusubov, M.S.; Resnati, G.; Postnikov, P.S.; Kukushkin, V.Y. Controlled Halogen-Bond-Involving Assembly of Double-σ-Hole-Donating Diaryliodonium Cations and Ditopic Arene Sulfonates. *Cryst. Growth Des.* **2023**, *23*, 413–423. [CrossRef]
30. Hill, J.A.; Thompson, A.L.; Goodwin, A.L. Dicyanometallates as Model Extended Frameworks. *J. Am. Chem. Soc.* **2016**, *138*, 5886–5896. [CrossRef]
31. Marinescu, G.; Madalan, A.M.; Andruh, M. New Heterometallic Coordination Polymers Based on Zinc(II) Complexes with Schiff-base Ligands and Dicyanometallates: Synthesis, Crystal Structures, and Luminescent Properties. *J. Coord. Chem.* **2015**, *68*, 479–490. [CrossRef]
32. Vlček, A.; Orendáč, M.; Orendáčová, A.; Kajňaková, M.; Papageorgiou, T.; Chomič, J.; Černák, J.; Massa, W.; Feher, A. Magneto-structural Correlation in $Cu(NH_3)_2Ag_2(CN)_4$. Crystal Structure, Magnetic and Thermodynamic Properties of an S = 1/2 Low-dimensional Heisenberg Antiferromagnet. *Solid State Sci.* **2007**, *9*, 116–125. [CrossRef]
33. Jeong, A.R.; Shin, J.W.; Jeong, J.H.; Hayami, S.; Min, K.S. Synthesis and Characterization of Heterobimetallic Coordination Polymers Containing Chiral Nickel(II) Macrocycle and Silver(I) Cyanide. *J. Incl. Phenom. Macrocycl. Chem.* **2015**, *82*, 145–152. [CrossRef]
34. Cruz, C.; Galdames, J.; Camayo-Gutierrez, L.; Rouzières, M.; Mathonière, C.; Menéndez, N.; Audebrand, N.; Reyes-Lillo, S.E.; Clérac, R.; Venegas-Yazigi, D.; et al. Thermally and Photoinduced Spin-Crossover Behavior in Iron(II)–Silver(I) Cyanido-Bridged Coordination Polymers Bearing Acetylpyridine Ligands. *Inorg. Chem.* **2024**, *63*, 17561–17573. [CrossRef]
35. Hiiuk, V.M.; Shylin, S.I.; Barakhtii, D.D.; Korytko, D.M.; Kotsyubynsky, V.O.; Rotaru, A.; Shova, S.; Gural'skiy, I.Y.A. Two-Step Spin Crossover in Hofmann-Type Coordination Polymers $[Fe(2\text{-phenylpyrazine})_2\{M(CN)_2\}_2]$ (M = Ag, Au). *Inorg. Chem.* **2022**, *61*, 2093–2104. [CrossRef]
36. Shylin, S.I.; Kucheriv, O.I.; Shova, S.; Ksenofontov, V.; Tremel, W.; Gural'skiy, I.y.A. Hofmann-Like Frameworks $Fe(2\text{-methylpyrazine})_n[M(CN)_2]_2$ (M = Au, Ag): Spin-Crossover Defined by the Precious Metal. *Inorg. Chem.* **2020**, *59*, 6541–6549. [CrossRef] [PubMed]
37. Sirenko, V.Y.; Kucheriv, O.I.; Shova, S.; Shylin, S.I.; Ksenofontov, V.; Fritsky, I.O.; Tremel, W.; Gural'skiy, I.y.A. Nature of Cyanoargentate Bridges Defining Spin Crossover in New 2D Hofmann Clathrate Analogues. *Dalton Trans.* **2024**, *53*, 4251–4259. [CrossRef] [PubMed]
38. Kucheriv, O.I.; Shylin, S.I.; Sirenko, V.Y.; Ksenofontov, V.; Tremel, W.; Dascălu, I.-A.; Shova, S.; Gural'skiy, I.y.A. Four-Step Spin Crossover in a New Cyano-Bridged Iron-Silver Coordination Polymer. *Chem. Eur. J.* **2022**, *28*, e202200924. [CrossRef]
39. Nemec, I.; Zoufalý, P.; Jewula, P.; Antal, P.; Linert, W.; Herchel, R. Ion-pair Complexes of Schiff Base Fe(III) Cations and Complex Anions. *New J. Chem.* **2019**, *43*, 4937–4946. [CrossRef]
40. Korkmaz, N.; Aydın, A.; Karadağ, A.; Yanar, Y.; Maaşoğlu, Y.; Şahin, E.; Tekin, Ş. New Bimetallic Dicyanidoargentate(I)-based Coordination Compounds: Synthesis, Characterization, Biological Activities and DNA-BSA Binding Affinities. *Spectrochim. Acta Part A Mol. Biomol. Spectrosc.* **2017**, *173*, 1007–1022. [CrossRef]
41. Hsieh, A.J.; Chantawansri, T.L.; Hu, W.; Strawhecker, K.E.; Casem, D.T.; Eliason, J.K.; Nelson, K.A.; Parsons, E.M. New Insight into Microstructure-mediated Segmental Dynamics in Select Model Poly(urethane urea) Elastomers. *Polymer* **2014**, *55*, 1883–1892. [CrossRef]
42. Stender, M.; White-Morris, R.L.; Olmstead, M.M.; Balch, A.L. New Structural Features of Unsupported Chains of Metal Ions in Luminescent $[(NH_3)_4Pt][Au(CN)_2]_2 \cdot 1.5(H_2O)$ and Related Salts. *Inorg. Chem.* **2003**, *42*, 4504–4506. [CrossRef]
43. Stork, J.R.; Rios, D.; Pham, D.; Bicocca, V.; Olmstead, M.M.; Balch, A.L. Metal−Metal Interactions in Platinum(II)/Gold(I) or Platinum(II)/Silver(I) Salts Containing Planar Cations and Linear Anions. *Inorg. Chem.* **2005**, *44*, 3466–3472. [CrossRef] [PubMed]
44. Kappenstein, C.; Ouali, A.; Guerin, M.; Černák, J.; Chomič, J. Preparation, Structure and Properties of Dicyano Silver Complexes of the $M(en)_3Ag_2(CN)_4$ and $M(en)_2Ag_2(CN)_4$ Type. *Inorg. Chim. Acta* **1988**, *147*, 189–197. [CrossRef]
45. Nawaz, S.; Ghaffar, A.; Monim-ul-Mehboob, M.; Tahir, M.N.; Alotaibi, M.A.; Isab, A.A.; Ahmad, S. Synthesis and Crystal Structure of a Cyanido-bridged Copper(II)–Silver(I) Bimetallic Complex Containing a Trimeric $\{[Ag(CN)_2]^-\}_3$ anion, $[Cu(Dach)_2\text{-}Ag(CN)_2\text{-}Cu(Dach)_2][Ag(CN)_2]_3$ (Dach=*cis*-1,2-diaminocyclohexane). *Z. Naturforsch. B* **2017**, *72*, 43–47. [CrossRef]

46. Nicholas, A.D.; Bullard, R.M.; Pike, R.D.; Patterson, H.H. Photophysical Investigation of Silver/Gold Dicyanometallates and Tetramethylammonium Networks: An Experimental and Theoretical Investigation. *Eur. J. Inorg. Chem.* **2019**, *2019*, 956–962. [CrossRef]
47. Yoshida, Y.; Muroi, K.; Otsuka, A.; Saito, G.; Takahashi, M.; Yoko, T. 1-Ethyl-3-methylimidazolium Based Ionic Liquids Containing Cyano Groups: Synthesis, Characterization, and Crystal Structure. *Inorg. Chem.* **2004**, *43*, 1458–1462. [CrossRef] [PubMed]
48. Chen, Y.; Cheng, G.; Li, K.; Shelar, D.P.; Lu, W.; Che, C.-M. Phosphorescent Polymeric Nanomaterials with Metallophilic $d^{10}\cdots d^{10}$ Interactions Self-assembled from $[Au(NHC)_2]^+$ and $[M(CN)_2]^-$. *Chem. Sci.* **2014**, *5*, 1348–1353. [CrossRef]
49. Klapötke, T.M.; Krumm, B.; Mayer, P.; Piotrowski, H.; Schwab, I.; Vogt, M. Synthesis and Structures of Triorganotelluronium Pseudohalides. *Eur. J. Inorg. Chem.* **2002**, 2701–2709. [CrossRef]
50. Aakeroy, C.B.; Bryce, D.L.; Desiraju, G.R.; Frontera, A.; Legon, A.C.; Nicotra, F.; Rissanen, K.; Scheiner, S.; Terraneo, G.; Metrangolo, P.; et al. Definition of the Chalcogen Bond (IUPAC Recommendations 2019). *Pure Appl. Chem.* **2019**, *91*, 1889–1892. [CrossRef]
51. Mallah, E.; Sweidan, K.; Abu-Salem, Q.; Abu Dayyih, W.; Steimann, M. 2-Bromo-1,3-diisopropyl-4,5-dimethyl-1H-imidazol-3-ium Dicyanidoargentate. *Acta Crystallogr. E* **2012**, *68*, m17. [CrossRef]
52. Imakubo, T.; Sawa, H.; Kato, R. Novel Radical Cation Salts of Organic π-Donors Containing Iodine Atom(s): The First Application of Strong Intermolecular-I···X-(X = CN, halogen atom) Interaction to Molecular Conductors. *Synth. Met.* **1995**, *73*, 117–122. [CrossRef]
53. Christopherson, J.-C.; Potts, K.P.; Bushuyev, O.S.; Topić, F.; Huskić, I.; Rissanen, K.; Barrett, C.J.; Friščić, T. Assembly and Dichroism of a Four-component Halogen-bonded Metal–organic Cocrystal Salt Solvate Involving Dicyanoaurate(I) Acceptors. *Faraday Discuss.* **2017**, *203*, 441–457. [CrossRef] [PubMed]
54. Soldatova, N.S.; Radzhabov, A.D.; Ivanov, D.M.; Burguera, S.; Frontera, A.; Abramov, P.A.; Postnikov, P.S.; Kukushkin, V.Y. Key-to-lock Halogen Bond-based Tetragonal Pyramidal Association of Iodonium Cations with the Lacune Rims of Beta-octamolybdate. *Chem. Sci.* **2024**, *15*, 12459–12472. [CrossRef] [PubMed]
55. Suslonov, V.V.; Soldatova, N.S.; Ivanov, D.M.; Postnikov, P.S.; Gomila, R.M.; Frontera, A.; Semenov, A.V.; Kukushkin, V.Y.; Bokach, N.A. Interplay of a Nitro Group and Metal Ions: From Coordinative Binding to Noncovalent Semicoordination. *Inorg. Chem. Front.* **2024**, *11*, 3961–3974. [CrossRef]
56. Yunusova, S.N.; Novikov, A.S.; Bolotin, D.S.; Il'in, M.V. Iodonium Cation Stabilizes Square-planar Configuration of the Silver(I) Tetratriflate. *Inorg. Chim. Acta* **2024**, *568*, 122079. [CrossRef]
57. Bondi, A. van der Waals Volumes and Radii. *J. Phys. Chem.* **1964**, *68*, 441–451. [CrossRef]
58. Imakubo, T.; Shirahata, T.; Kibune, M.; Yoshino, H. Hybrid Organic/Inorganic Supramolecular Conductors $D_2[Au(CN)_4]$ [D = Diiodo(ethylenedichalcogeno)tetrachalcogenofulvalene], Including a New Ambient Pressure Superconductor. *Eur. J. Inorg. Chem.* **2007**, *2007*, 4727–4735. [CrossRef]
59. Imakubo, T.; Tajima, N.; Tamura, M.; Kato, R.; Nishio, Y.; Kajita, K. A Supramolecular Superconductor θ-$(DIETS)_2[Au(CN)_4]$. *J. Mater. Chem.* **2002**, *12*, 159–161. [CrossRef]
60. Ormond-Prout, J.E.; Smart, P.; Brammer, L. Cyanometallates as Halogen Bond Acceptors. *Cryst. Growth Des.* **2012**, *12*, 205–216. [CrossRef]
61. Jakupec, N.; Fotović, L.; Stilinović, V. The Effect of Halogen Bonding on Protonated Hexacyanoferrate Networks in Hexacyanoferrates of Halogenopyridines. *CrystEngComm* **2020**, *22*, 8142–8150. [CrossRef]
62. Sellin, M.; Rupf, S.M.; Zhang, Y.; Malischewski, M. Bi- and Trifurcated Halogen Bonding M–C≡N···I in 1D, 2D, and 3D Supramolecular Network Structures of Co-Crystallized Diiodoacetylene C_2I_2 and Tetracyanonickelate $[Ni(CN)_4]^{2-}$. *Cryst. Growth Des.* **2020**, *20*, 7104–7110. [CrossRef]
63. Sellin, M.; Rupf, S.M.; Malischewski, M. Cubic Three-Dimensional Networks of the Cyanometalate $[Fe(CN)_6]^{3-}$ with the Ditopic Halogen Bond Donor Diiodoacetylene C_2I_2. *Cryst. Growth Des.* **2021**, *21*, 5515–5520. [CrossRef]
64. Lippert, G.; Hutter, J.; Parrinello, M. The Gaussian and Augmented-plane-wave Density Functional Method for *ab initio* Molecular Dynamics Simulations. *Theor. Chem. Acc.* **1999**, *103*, 124–140. [CrossRef]
65. Johnson, E.R.; Keinan, S.; Mori-Sanchez, P.; Contreras-Garcia, J.; Cohen, A.J.; Yang, W.T. Revealing Noncovalent Interactions. *J. Am. Chem. Soc.* **2010**, *132*, 6498–6506. [CrossRef]
66. Espinosa, E.; Alkorta, I.; Elguero, J.; Molins, E. From Weak to Strong Interactions: A Comprehensive Analysis of the Topological and Energetic Properties of the Electron Density Distribution Involving X−H···F−Y Systems. *J. Chem. Phys.* **2002**, *117*, 5529–5542. [CrossRef]
67. Becke, A.D.; Edgecombe, K.E. A Simple Measure of Electron Localization in Atomic And Molecular Systems. *J. Chem. Phys.* **1990**, *92*, 5397–5403. [CrossRef]
68. Silvi, B.; Savin, A. Classification of Chemical Bonds Based on Topological Analysis of Electron Localization Functions. *Nature* **1994**, *371*, 683–686. [CrossRef]
69. Savin, A.; Nesper, R.; Wengert, S.; Fassler, T.F. ELF: The Electron Localization Function. *Angew. Chem. Int. Ed.* **1997**, *36*, 1809–1832. [CrossRef]

70. Bartashevich, E.V.; Matveychuk, Y.V.; Troitskaya, E.A.; Tsirelson, V.G. Characterizing the Multiple Non-covalent Interactions in N, S-heterocycles–Diiodine Complexes with Focus on Halogen Bonding. *Comput. Theor. Chem.* **2014**, *1037*, 53–62. [CrossRef]
71. Bartashevich, E.; Yushina, I.; Kropotina, K.; Muhitdinova, S.; Tsirelson, V. Testing the Tools for Revealing and Characterizing the Iodine-Iodine Halogen Bond in Crystals. *Acta Crystallogr. Sect. B* **2017**, *73*, 217–226. [CrossRef]
72. Lamberts, K.; Handels, P.; Englert, U.; Aubert, E.; Espinosa, E. Stabilization of Polyiodide Chains via Anion· · · Anion Interactions: Experiment and Theory. *CrystEngComm* **2016**, *18*, 3832–3841. [CrossRef]
73. Bartashevich, E.; Mukhitdinova, S.; Yushina, I.; Tsirelson, V. Electronic Criterion for Categorizing the Chalcogen and Halogen Bonds: Sulfur–Iodine Interactions in Crystals. *Acta Crystallogr. Sect. B* **2019**, *75*, 117–126. [CrossRef] [PubMed]
74. Bartashevich, E.; Matveychuk, Y.; Tsirelson, V. Identification of the Tetrel Bonds between Halide Anions and Carbon Atom of Methyl Groups Using Electronic Criterion. *Molecules* **2019**, *24*, 1083. [CrossRef]
75. Mata, I.; Molins, E.; Alkorta, I.; Espinosa, E. Topological Properties of the Electrostatic Potential in Weak and Moderate N···H Hydrogen Bonds. *J. Phys. Chem. A* **2007**, *111*, 6425–6433. [CrossRef]
76. Bulatova, M.; Ivanov, D.M.; Rautiainen, J.M.; Kinzhalov, M.A.; Truong, K.-N.; Lahtinen, M.; Haukka, M. Studies of Nature of Uncommon Bifurcated I–I···(I–M) Metal-Involving Noncovalent Interaction in Palladium(II) and Platinum(II) Isocyanide Cocrystals. *Inorg. Chem.* **2021**, *60*, 13200–13211. [CrossRef]
77. Podrezova, E.V.; Okhina, A.A.; Rogachev, A.D.; Baykov, S.V.; Kirschning, A.; Yusubov, M.S.; Soldatova, N.S.; Postnikov, P.S. Ligand-free Ullmann-type Arylation of Oxazolidinones by Diaryliodonium Salts. *Org. Biomol. Chem.* **2023**, *21*, 1952–1957. [CrossRef]
78. Palatinus, L.; Chapuis, G. SUPERFLIP—A Computer Program for the Solution of Crystal Structures by Charge Flipping in Arbitrary Dimensions. *J. Appl. Crystallogr.* **2007**, *40*, 786–790. [CrossRef]
79. Palatinus, L.; Prathapa, S.J.; van Smaalen, S. EDMA: A Computer Program for Topological Analysis of Discrete Electron Densities. *J. Appl. Crystallogr.* **2012**, *45*, 575–580. [CrossRef]
80. Palatinus, L.; van der Lee, A. Symmetry Determination Following Structure Solution in P1. *J. Appl. Crystallogr.* **2008**, *41*, 975–984. [CrossRef]
81. Sheldrick, G.M. SHELXT—Integrated Space-group and Crystal Structure Determination. *Acta Crystallogr. Sect. A* **2015**, *71*, 3–8. [CrossRef]
82. Dolomanov, O.V.; Bourhis, L.J.; Gildea, R.J.; Howard, J.A.K.; Puschmann, H. OLEX2: A Complete Structure Solution, Refinement and Analysis Program. *J. Appl. Crystallogr.* **2009**, *42*, 339–341. [CrossRef]
83. Allen, F.H.; Bruno, I.J. Bond Lengths in Organic and Metal-organic Compounds Revisited: X–H Bond Lengths from Neutron Diffraction Data. *Acta Cryst. B* **2010**, *66*, 380–386. [CrossRef]
84. Frigo, M.; Johnson, S.G. The Design and Implementation of FFTW3. *Proc. IEEE* **2005**, *93*, 216–231. [CrossRef]
85. VandeVondele, J.; Krack, M.; Mohamed, F.; Parrinello, M.; Chassaing, T.; Hutter, J. Quickstep: Fast and Accurate Density Functional Calculations Using a Mixed Gaussian and Plane Waves Approach. *Comput. Phys. Comm.* **2005**, *167*, 103–128. [CrossRef]
86. Hutter, J.; Iannuzzi, M.; Schiffmann, F.; VandeVondele, J. cp2k: Atomistic Simulations of Condensed Matter Systems. *WIREs Comput. Mol. Sci.* **2014**, *4*, 15–25. [CrossRef]
87. Borštnik, U.; VandeVondele, J.; Weber, V.; Hutter, J. Sparse Matrix Multiplication: The Distributed Block-compressed Sparse Row Library. *Parallel Comput.* **2014**, *40*, 47–58. [CrossRef]
88. Schütt, O.; Messmer, P.; Hutter, J.; VandeVondele, J. GPU-Accelerated Sparse Matrix–Matrix Multiplication for Linear Scaling Density Functional Theory. In *Electronic Structure Calculations on Graphics Processing Units*; Wiley & Sons, Inc.: Hoboken, NJ, USA, 2016; pp. 173–190. [CrossRef]
89. Goerigk, L.; Hansen, A.; Bauer, C.; Ehrlich, S.; Najibi, A.; Grimme, S. A Look at the Density Functional Theory Zoo with the Advanced GMTKN55 Database for General Main Group Thermochemistry, Kinetics and Noncovalent Interactions. *Phys. Chem. Chem. Phys.* **2017**, *19*, 32184–32215. [CrossRef] [PubMed]
90. Kühne, T.D.; Iannuzzi, M.; Del Ben, M.; Rybkin, V.V.; Seewald, P.; Stein, F.; Laino, T.; Khaliullin, R.Z.; Schütt, O.; Schiffmann, F.; et al. CP2K: An Electronic Structure and Molecular Dynamics Software Package—Quickstep: Efficient and Accurate Electronic Structure Calculations. *J. Chem. Phys.* **2020**, *152*, 194103. [CrossRef] [PubMed]
91. Perdew, J.P.; Burke, K.; Ernzerhof, M. Generalized Gradient Approximation Made Simple. *Phys. Rev. Lett.* **1996**, *77*, 3865–3868. [CrossRef]
92. Grimme, S.; Antony, J.; Ehrlich, S.; Krieg, H. A Consistent And Accurate *ab initio* Parametrization of Density Functional Dispersion Correction (DFT-D) for the 94 Elements H-Pu. *J. Chem. Phys.* **2010**, *132*, 154104. [CrossRef]
93. Grimme, S.; Ehrlich, S.; Goerigk, L. Effect of the Damping Function in Dispersion Corrected Density Functional Theory. *J. Comput. Chem.* **2011**, *32*, 1456–1465. [CrossRef]
94. Jorge, F.E.; Canal Neto, A.; Camiletti, G.G.; Machado, S.F. Contracted Gaussian Basis Sets for Douglas–Kroll–Hess Calculations: Estimating Scalar Relativistic Effects of Some Atomic and Molecular Properties. *J. Chem. Phys.* **2009**, *130*, 064108. [CrossRef]

95. Barros, C.L.; de Oliveira, P.J.P.; Jorge, F.E.; Canal Neto, A.; Campos, M. Gaussian Basis Set of Double Zeta Quality for Atoms Rb through Xe: Application in Non-relativistic and Relativistic Calculations of Atomic and Molecular Properties. *Mol. Phys.* **2010**, *108*, 1965–1972. [CrossRef]
96. de Berrêdo, R.C.; Jorge, F.E. All-electron Double Zeta Basis Sets for Platinum: Estimating Scalar Relativistic Effects on Platinum(II) Anticancer Drugs. *J. Mol. Struct. THEOCHEM* **2010**, *961*, 107–112. [CrossRef]
97. Pritchard, B.P.; Altarawy, D.; Didier, B.; Gibson, T.D.; Windus, T.L. New Basis Set Exchange: An Open, Up-to-Date Resource for the Molecular Sciences Community. *J. Chem. Inf. Model.* **2019**, *59*, 4814–4820. [CrossRef]
98. Barysz, M.; Sadlej, A.J. Two-component Methods of Relativistic Quantum Chemistry: From the Douglas-Kroll Approximation to the Exact Two-component Formalism. *J. Mol. Struct. THEOCHEM* **2001**, *573*, 181–200. [CrossRef]
99. Reiher, M. Relativistic Douglas–Kroll–Hess theory. *WIREs Comput. Mol. Sci.* **2012**, *2*, 139–149. [CrossRef]
100. Frisch, M.J.T.; Trucks, G.W.; Schlegel, H.B.; Scuseria, G.E.; Robb, M.A.; Cheeseman, J.R.; Scalmani, G.; Barone, V.; Petersson, G.A.; Nakatsuji, H.; et al. *Gaussian 09, Revision C.01*; Gaussian, Inc.: Wallingford, CT, USA, 2010.
101. Bader, R.F.W. A Quantum Theory of Molecular Structure and its Applications. *Chem. Rev.* **1991**, *91*, 893–928. [CrossRef]
102. Lu, T.; Chen, F.W. Multiwfn: A Multifunctional Wavefunction Analyzer. *J. Comput. Chem.* **2012**, *33*, 580–592. [CrossRef]
103. McKinnon, J.J.; Jayatilaka, D.; Spackman, M.A. Towards Quantitative Analysis of Intermolecular Interactions with Hirshfeld Surfaces. *Chem. Comm.* **2007**, *37*, 3814–3816. [CrossRef]
104. Spackman, P.R.; Turner, M.J.; McKinnon, J.J.; Wolff, S.K.; Grimwood, D.J.; Jayatilaka, D.; Spackman, M.A. CrystalExplorer: A Program for Hirshfeld Surface Analysis, Visualization and Quantitative Analysis of Molecular Crystals. *J. Appl. Crystallogr.* **2021**, *54*, 1006–1011. [CrossRef]
105. Spackman, M.A.; Jayatilaka, D. Hirshfeld Surface Analysis. *CrystEngComm* **2009**, *11*, 19–32. [CrossRef]

Disclaimer/Publisher's Note: The statements, opinions and data contained in all publications are solely those of the individual author(s) and contributor(s) and not of MDPI and/or the editor(s). MDPI and/or the editor(s) disclaim responsibility for any injury to people or property resulting from any ideas, methods, instructions or products referred to in the content.